A posteriori local subcell correction of high-order DG schemes on unstructured grids

François Vilar[1] and **Rémi Abgrall**[2]

[1]Institut Montpelliérain Alexander Grothendieck, Université de Montpellier

[2]Institut für Mathematik, Universität Zürich

October 2022

Scalar conservation law

- $\partial_t u(\mathbf{x},t) + \nabla_x . \mathbf{F}(u(\mathbf{x},t)) = 0, \qquad (\mathbf{x},t) \in \omega \times [0,T]$
- $u(\mathbf{x},0) = u_0(\mathbf{x}), \qquad \mathbf{x} \in \omega$

$(k+1)^{\text{th}}$ order semi-discretization

- $\{\omega_c\}_c$ a partition of ω, such that $\omega = \bigcup_c \omega_c$
- $u_h(\mathbf{x},t)$ the numerical solution, such that $u_{h|\omega_c} = u_h^c \in \mathbb{P}^k(\omega_c)$

$$u_h^c(\mathbf{x},t) = \sum_{m=1}^{N_k} u_m^c(t)\,\sigma_m^c(\mathbf{x})$$

- $\{\sigma_m^c\}_{m=1,\dots,N_k}$ a basis of $\mathbb{P}^k(\omega_c)$, with $N_k = \frac{(k+1)(k+2)}{2}$ in 2D.

Local variational formulation on ω_c

- $\displaystyle\int_{\omega_c} \frac{\partial u_h^c}{\partial t}\,\psi\,\mathrm{d}V = \int_{\omega_c} \mathbf{F}(u_h^c) . \nabla_x \psi\,\mathrm{d}V - \int_{\partial\omega_c} \psi\,\mathcal{F}_n\,\mathrm{d}S, \qquad \forall\,\psi \in \mathbb{P}^k(\omega_c)$
- $\mathcal{F}_n = \mathcal{F}\left(u_h^c, u_h^v, \mathbf{n}\right)$ numerical flux

Numerical example: solid body rotation

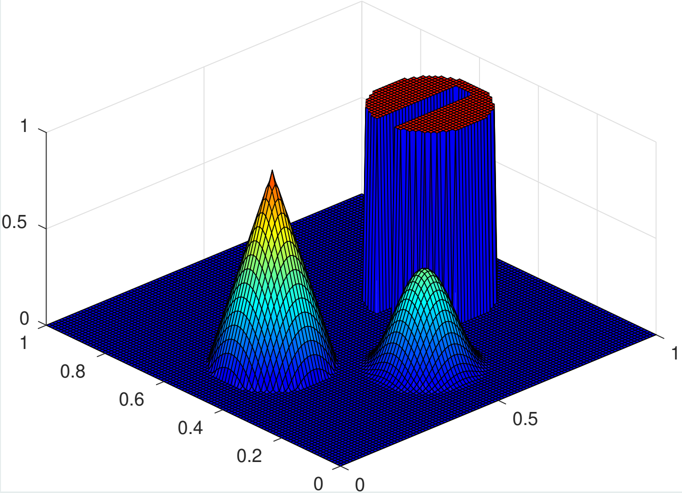

Figure : Rotation of composite signal: initial solution

Roughly constant number of degrees of freedom

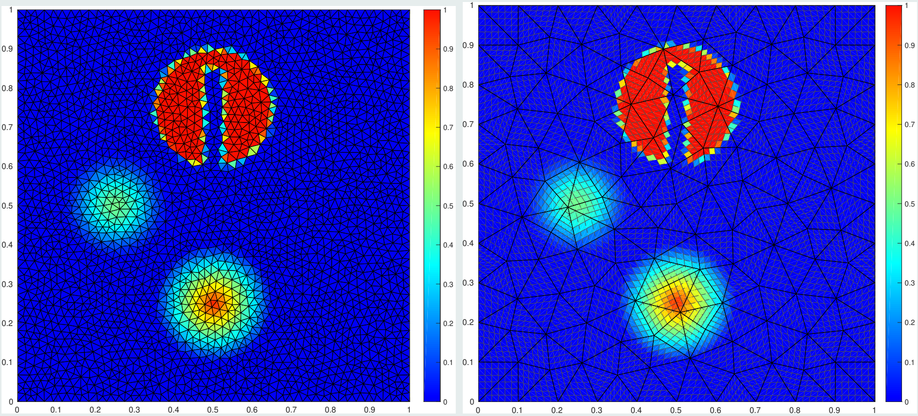

(a) 1st order on 5154 cells

(b) 6th order on 242 cells (5082 DoF)

Figure : Rotation of composite signal: initial solution

Subcell resolution of DG scheme

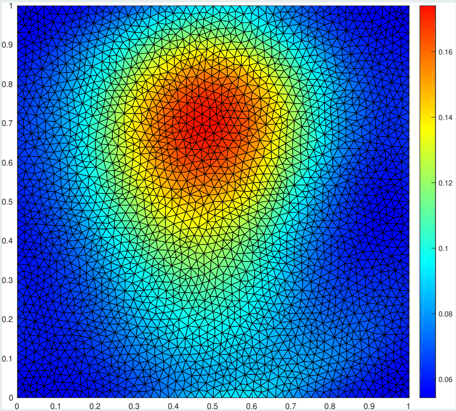

(c) 1st order on 5154 cells

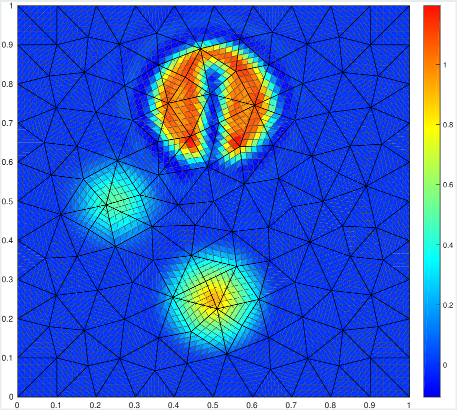

(d) 6th order on 242 cells (5082 DoF)

Figure : Rotation of composite signal after one period: subcells mean value

Subcell resolution of DG scheme

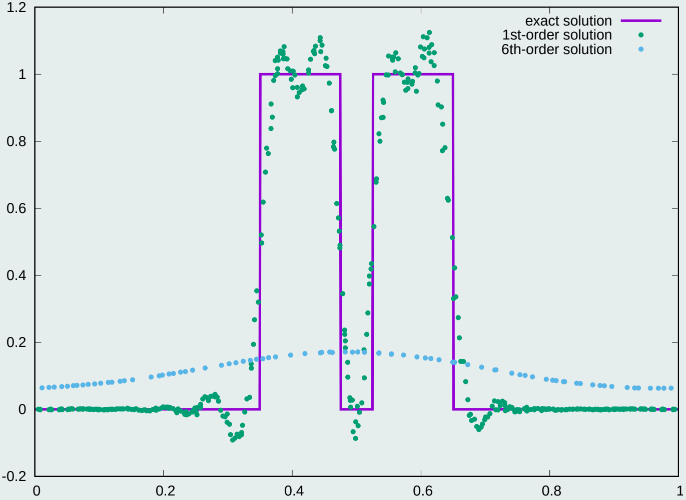

Figure : Rotation of composite signal after one period: profiles for $y = 0.75$

Admissible numerical solution

- Maximum principle / positivity preserving
- Prevent the code from crashing (for instance avoiding NaN)
- **Ensure the conservation of the scheme**

Spurious oscillations

- Discrete maximum principle
- Relaxing condition for smooth extrema

Accuracy

- Retain as much as possible the subcell resolution of the DG scheme
- Minimize the number of subcell solutions to recompute

Modify locally, at the subcell level, the numerical solution without impacting the solution elsewhere in the cell

F. VILAR, *A Posteriori Correction of High-Order DG Scheme through Subcell Finite Volume Formulation and Flux Reconstruction.* JCP, 2018.

DG as a subcell Finite Volume

- Rewrite DG scheme as a FV-like scheme on a subgrid

Cell subdivision into N_k subcells

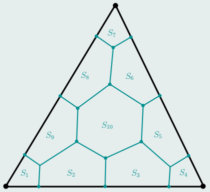

Figure : Examples of subdivision for a $\mathbb{P}^3$ DG scheme on a triangular cell

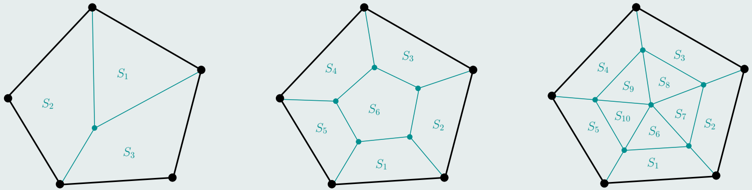

Figure : Examples of subdivision for a polygonal cell from $\mathbb{P}^1$ up to $\mathbb{P}^3$

DG schemes through residuals

- $$\sum_{m=1}^{N_k} \frac{\mathrm{d}\, u_m^c}{\mathrm{d}t} \int_{\omega_c} \sigma_m \, \sigma_p \, \mathrm{d}V = \int_{\omega_c} \mathbf{F}(u_h^c) \,\boldsymbol{.}\, \nabla_x \sigma_p \, \mathrm{d}V - \int_{\partial\omega_c} \sigma_p \, \mathcal{F}_n \, \mathrm{d}S, \quad \forall\, p \in [\![1, N_k]\!]$$

$$\Longrightarrow \qquad \boxed{M_c \, \frac{\mathrm{d}\, U_c}{\mathrm{d}t} = \Phi_c}$$

- $(U_c)_m = u_m^c$ — Solution moments
- $(M_c)_{mp} = \displaystyle\int_{\omega_c} \sigma_m \, \sigma_p \, \mathrm{d}V$ — Mass matrix
- $(\Phi_c)_m = \displaystyle\int_{\omega_c} \mathbf{F}(u_h^c) \,\boldsymbol{.}\, \nabla_x \sigma_m \, \mathrm{d}V - \int_{\partial\omega_c} \sigma_m \, \mathcal{F}_n \, \mathrm{d}S$ — DG residuals

Subdivision and definition

- ω_c is subdivided into N_k subcells S_m^c
- Let us define $\displaystyle \overline{\psi}_m^c = \frac{1}{|S_m^c|} \int_{S_m^c} \psi \, \mathrm{d}V$ the subcell mean value

Submean values

- $$\frac{\mathrm{d}\,\overline{u}_m^c}{\mathrm{d}t} = \frac{1}{|S_m^c|} \sum_{q=1}^{N_k} \frac{\mathrm{d}\,u_q^c}{\mathrm{d}t} \int_{S_m^c} \sigma_q \,\mathrm{d}V$$

$$\Longrightarrow \quad \boxed{\frac{\mathrm{d}\,\overline{U}_c}{\mathrm{d}t} = P_c \frac{\mathrm{d}\,U_c}{\mathrm{d}t}}$$

- $(\overline{U}_c)_m = \overline{u}_m^c$ Submean values
- $(P_c)_{mp} = \dfrac{1}{|S_m^c|} \displaystyle\int_{S_m^c} \sigma_p \,\mathrm{d}V$ Projection matrix

$$\Longrightarrow \quad \boxed{\frac{\mathrm{d}\,\overline{U}_c}{\mathrm{d}t} = P_c\, M_c^{-1}\, \Phi_c}$$

Admissibility of the cell sub-partition into subcells

- P_c **has to be non-singular**

Subcell Finite Volume: reconstructed fluxes

- Let us introduce the **reconstructed fluxes** such that

$$\boxed{\frac{\mathrm{d}\,\overline{u}_m^c}{\mathrm{d}t} = -\frac{1}{|S_m^c|}\int_{\partial S_m^c} \widehat{F}_n \,\mathrm{d}S}$$

- Let $\mathcal{V}_m^c$ be the set of face neighboring subcells of S_m^c

$$\frac{\mathrm{d}\,\overline{u}_m^c}{\mathrm{d}t} = -\frac{1}{|S_m^c|}\sum_{S_p^v \in \mathcal{V}_m^c}\int_{f_{mp}^c} \widehat{F}_n \,\mathrm{d}S$$

- We impose that on the boundary of cell ω_c

$$\boxed{\widehat{F}_{n|_{\partial\omega_c}} = \mathcal{F}_n}$$

- Then, if $\widetilde{\mathcal{V}_m^c}$ stands for the set of face neighboring subcells inside ω_c

$$\frac{\mathrm{d}\,\overline{u}_m^c}{\mathrm{d}t} = -\frac{1}{|S_m^c|}\left(\sum_{S_p^c \in \widetilde{\mathcal{V}_m^c}}\int_{f_{mp}^c} \widehat{F}_n \,\mathrm{d}S + \int_{\partial S_m^c \cap \partial\omega_c} \mathcal{F}_n \,\mathrm{d}S\right)$$

Subcell Finite Volume: reconstructed fluxes

- Taking two subcells S_m^c and S_p^v, the orientation face function ε_{mp}^c writes

$$\varepsilon_{mp}^c = \begin{cases} 1 & \text{if face } f_{mp}^c \text{ is direct or if } f_{mp}^c \subset \partial\omega_c, \\ -1 & \text{if face } f_{mp}^c \text{ is indirect,} \\ 0 & \text{if } S_p^v \notin \mathcal{V}_m^c. \end{cases}$$

- $\displaystyle\int_{f_{mp}^c} \widehat{F_n}\,\mathrm{d}S = \varepsilon_{mp}^c\,\widehat{F_{mp}}$ face integrated reconstructed flux

$$\boxed{\frac{\mathrm{d}\,\overline{u}_m^c}{\mathrm{d}t} = -\frac{1}{|S_m^c|}\left(\sum_{S_p^c \in \mathcal{V}_m^c} \varepsilon_{mp}^c\,\widehat{F_{mp}} + \int_{\partial S_m^c \cap \partial\omega_c} \mathcal{F}_n\,\mathrm{d}S\right)}$$

- $(B_c)_m = \displaystyle\int_{\partial S_m^c \cap \partial\omega_c} \mathcal{F}_n\,\mathrm{d}S$ Cell boundary contribution
- $(A_c)_{mp} = \varepsilon_{mp}^c$ Adjacency matrix
- $D_c = \mathrm{diag}\left(|S_1^c|, \dots, |S_{N_k}^c|\right)$ Subcells volume matrix

Subcell Finite Volume: reconstructed fluxes

- Let $\widehat{F_c}$ be the vector containing all the interior faces reconstructed fluxes
- The subcell mean values governing equations yield the following system

$$\boxed{-A_c\,\widehat{F_c} = D_c\,\frac{\mathrm{d}\,\overline{U}_c}{\mathrm{d}t} + B_c}$$

Graph Laplacian technique

- $A_c \in \mathcal{M}_{N_k \times N_f^c}$ with N_f^c the number of interior faces
- $A_c^{\mathrm{t}}\,\mathbf{1} = \mathbf{0}$ where $\mathbf{1} = (1, \ldots, 1)^{\mathrm{t}} \in \mathbb{R}^{N_k}$

R. Abgrall, *Some Remarks about Conservation for Residual Distribution Schemes.* Methods Appl. Math., 18:327-351, 2018.

- Let $\mathcal{L}_c^{-1}$ be the inverse of $L_c = A_c\,A_c^{\mathrm{t}}$ on the orthogonal of its kernel

$$\boxed{\mathcal{L}_c^{-1} = (L_c + \lambda\,\Pi)^{-1} - \frac{1}{\lambda}\,\Pi} \qquad \forall\lambda \neq 0$$

- $\Pi = \frac{1}{N_k}\,(\mathbf{1} \otimes \mathbf{1}) \in \mathcal{M}_{N_k}$

Graph Laplacian technique

- Finally, we obtain the following definition of the reconstructed fluxes

$$\boxed{\widehat{F_c} = -A_c^{\mathrm{t}}\,\mathcal{L}_c^{-1}\left(D_c\,P_c\,M_c^{-1}\,\Phi_c + B_c\right)}$$

remark

- The only terms depending on the time are Φ_c and B_c

Back to the DG scheme

- The polynomial solution is defined through reconstructed fluxes as follows

$$\boxed{\frac{\mathrm{d}\,U_c}{\mathrm{d}t} = -P_c^{-1}\,D_c^{-1}\left(A_c\,\widehat{F_c} + B_c\right)}$$

Question

- Is the reconstructed flux $\widehat{F_c}$ close to the interior flux $\boldsymbol{F}(u_h^c)$?

Local variational formulation

- $$\int_{\omega_c} \frac{\partial u_h^c}{\partial t}\, \psi \,\mathrm{d}V = \int_{\omega_c} \mathbf{F}(u_h^c) \,.\, \nabla_x \psi \,\mathrm{d}V - \int_{\partial\omega_c} \psi\, \mathcal{F}_n \,\mathrm{d}S, \qquad \forall\, \psi \in \mathbb{P}^k(\omega_c)$$
- Substitute $\boldsymbol{F}(u_h^c)$ with $\boldsymbol{F}_h^c \in \left(\mathbb{P}^{k+1}(\omega_c)\right)^2$ (collocated or L_2 projection)
- $$\int_{\omega_c} \frac{\partial u_h^c}{\partial t}\, \psi \,\mathrm{d}V = -\int_{\omega_c} \psi\, \nabla_x \,.\, \boldsymbol{F}_h^c \,\mathrm{d}V + \int_{\partial\omega_c} \psi \left(\boldsymbol{F}_h^c \,.\, \boldsymbol{n} - \mathcal{F}_n\right) \mathrm{d}S, \quad \forall\, \psi \in \mathbb{P}^k(\omega_c)$$

Subresolution basis functions

- Let us introduce the N_k basis functions $\{\phi_m\}_m$ such that $\forall\, \psi \in \mathbb{P}^k(\omega_c)$

$$\int_{\omega_c} \phi_m\, \psi \,\mathrm{d}V = \int_{S_m^c} \psi \,\mathrm{d}V, \qquad \forall\, m = 1, \ldots, N_k,$$

- $$\sum_{m=1}^{N_k} \phi_m(\boldsymbol{x}) = 1$$

$$\boxed{\text{These particular functions can be seen as the } L_2 \text{ projection of the indicator functions } \mathbb{1}_m(\boldsymbol{x}) \text{ onto } \mathbb{P}^k(\omega_c)}$$

Subcell Finite Volume scheme

- $$\int_{\omega_c} \frac{\partial u_h^c}{\partial t}\, \phi_m \,\mathrm{d}V = -\int_{\omega_c} \phi_m \,\nabla_x \cdot \boldsymbol{F}_h^c \,\mathrm{d}V + \int_{\partial\omega_c} \phi_m \,\left(\boldsymbol{F}_h^c \cdot \boldsymbol{n} - \mathcal{F}_n\right) \mathrm{d}S$$
- $$|S_m^c| \frac{\mathrm{d}\,\overline{u}_m^c}{\mathrm{d}t} = -\int_{S_m^c} \nabla_x \cdot \boldsymbol{F}_h^c \,\mathrm{d}V + \int_{\partial\omega_c} \phi_m \,\left(\boldsymbol{F}_h^c \cdot \boldsymbol{n} - \mathcal{F}_n\right) \mathrm{d}S$$
- $$\frac{\mathrm{d}\,\overline{u}_m^c}{\mathrm{d}t} = -\frac{1}{|S_m^c|}\left(\int_{\partial S_m^c} \boldsymbol{F}_h^c \cdot \boldsymbol{n} \,\mathrm{d}S - \int_{\partial\omega_c} \phi_m \,\left(\boldsymbol{F}_h^c \cdot \boldsymbol{n} - \mathcal{F}_n\right) \mathrm{d}S\right)$$
- $$\frac{\mathrm{d}\,\overline{u}_m^c}{\mathrm{d}t} = -\frac{1}{|S_m^c|}\int_{\partial S_m^c} \widehat{F_n} \,\mathrm{d}S$$ Subcell Finite Volume

Reconstructed Fluxes

- Finally, we get that

$$\boxed{\int_{\partial S_m^c} \widehat{F_n} \,\mathrm{d}S = \int_{\partial S_m^c} \boldsymbol{F}_h^c \cdot \boldsymbol{n} \,\mathrm{d}S - \int_{\partial\omega_c} \phi_m \,\left(\boldsymbol{F}_h^c \cdot \boldsymbol{n} - \mathcal{F}_n\right) \mathrm{d}S}$$

Reconstructed fluxes

- As we impose that $\widehat{F_n}_{|\partial\omega_c} = \mathcal{F}_n$, this last expression rewrites

$$\int_{\partial S_m^c \setminus \partial\omega_c} \widehat{F_n}\,\mathrm{d}S = \int_{\partial S_m^c \setminus \partial\omega_c} \boldsymbol{F}_h^c \,.\, \boldsymbol{n}\,\mathrm{d}S - \int_{\partial\omega_c} \widetilde{\phi_m}\, \left(\boldsymbol{F}_h^c \,.\, \boldsymbol{n} - \mathcal{F}_n\right)\,\mathrm{d}S$$

- $\widetilde{\phi_m} = \begin{cases} \phi_m & \text{if } \boldsymbol{x} \in \partial\omega_c \setminus \partial S_m^c \\ \phi_m - 1 & \text{if } \boldsymbol{x} \in \partial\omega_c \bigcap \partial S_m^c \end{cases}$

- $\displaystyle\int_{f_{mp}^c} \widehat{F_n}\,\mathrm{d}S = \varepsilon_{mp}^c\,\widehat{F_{mp}}$ and $\displaystyle\int_{f_{mp}^c} \boldsymbol{F}_h^c \,.\, \boldsymbol{n}\,\mathrm{d}S = \varepsilon_{mp}^c\,F_{mp}$

- Then, if F_c is the vector containing all the interior faces fluxes, one gets

$$\boxed{A_c\,\widehat{F_c} = A_c\,F_c - G_c}$$

- $(G_c)_m = \displaystyle\int_{\partial\omega_c} \widetilde{\phi_m}\, \left(\boldsymbol{F}_h^c \,.\, \boldsymbol{n} - \mathcal{F}_n\right)\,\mathrm{d}S$ Boundary contribution

Reconstructed fluxes through interior fluxes

- Making use of the same graph Laplacian technique, we finally obtain

$$\boxed{\widehat{F_c} = F_c - A_c^{\mathrm{t}}\, \mathcal{L}_c^{-1}\, G_c}$$

- We can rewrite this expression as

$$\widehat{F_c} = F_c - \mathcal{G}\big(\boldsymbol{F}_h^c \boldsymbol{.}\, \boldsymbol{n} - \mathcal{F}_n\big)$$

where $\mathcal{G}(.)$ is a correction function taking into account the jump between the polynomial flux and the numerical flux on the cell boundary

Remark

- Different choice in the correction term $\mathcal{G}(.)$ leads to different schemes
- For instance, $\mathcal{G}(.) = 0$ leads to the spectral volume scheme of Z.J. Wang

RKDG scheme

- SSP Runge-Kutta: convex combinations of first-order forward Euler
- For sake of clarity, we focus on forward Euler time stepping

Projection on subcells of RKDG solution

- $u_h^{c,n}(x) = \displaystyle\sum_{m=1}^{N_k} u_m^{c,n}\,\sigma_m(x)$
- $u_h^{c,n}$ is uniquely defined by its N_k submean values $\overline{u}_m^{c,n}$
- Recalling the definition of the projection matrix $(P_c)_{mp} = \dfrac{1}{|S_m^c|}\displaystyle\int_{S_m^c} \sigma_p \,\mathrm{d}V,$

$$\Longrightarrow \qquad P_c \begin{pmatrix} u_1^{c,n} \\ \vdots \\ u_{N_k}^{c,n} \end{pmatrix} = \begin{pmatrix} \overline{u}_1^{c,n} \\ \vdots \\ \overline{u}_{N_k}^{c,n} \end{pmatrix}$$

Set up

- We assume that, for each cell, the $\{\overline{u}_m^{c,n}\}_m$ are admissible
- Compute a candidate solution u_h^{n+1} from u_h^n through uncorrected DG
- For each subcell, check if the submean values $\{\overline{u}_m^{c,n+1}\}_m$ are OK

Physical admissibility detection (PAD)

- Check if $\overline{u}_m^{c,n+1}$ lies in an convex physical admissible set (maximum principle for SCL, positivity of the pressure and density for Euler, ...)
- Check if there is any *NaN* values

Numerical admissibility detection (NAD)

- Discrete maximum principle DMP on submean values:

$$\min_{v\in\mathcal{V}(S_m^c)} \left(\overline{u}_v^n\right) \le \overline{u}_m^{c,n+1} \le \max_{v\in\mathcal{V}(S_m^c)} \left(\overline{u}_v^n\right)$$

- $\mathcal{V}(S_m^c)$ set of neighboring subcells of S_m^c, including subcell S_m^c
- **This criterion needs to be relaxed to preserve smooth extrema**

Fundamental principle

- On non-admissible subcell boundaries

Substitute the reconstructed fluxes by more robust numerical fluxes

- Recompute the non-admissible subcells, and their first neighbors

Examples of correction schemes

- **1st-order Finite Volume scheme**
- 2nd-order MUSCL scheme
- (W)ENO methods
- . . .

Corrected reconstructed flux

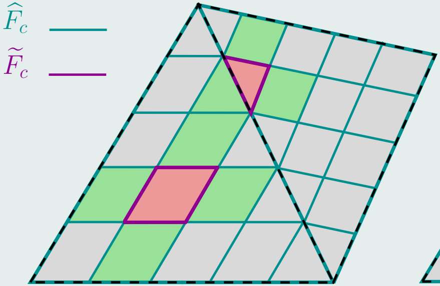

(d) Structured subdivision.

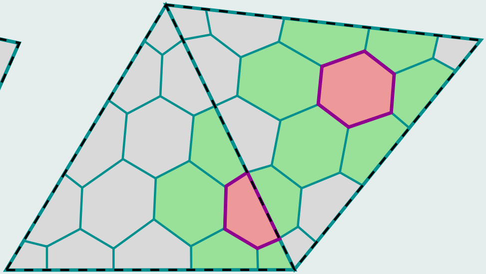

(e) Voronoi-type subdivision.

Figure : Original correction of the DG reconstructed flux

Flowchart

1. Compute the uncorrected DG candidate solution $u_h^{c,n+1}$
2. Project $u_h^{c,n+1}$ to get the submean values $\overline{u}_m^{c,n+1}$
3. Check $\overline{u}_m^{c,n+1}$ through the troubled zone detection plus relaxation
4. If $\overline{u}_m^{c,n+1}$ is admissible, go further in time. Otherwise, if S_m^c or $S_p^v \in \mathcal{V}_m^c$ is either marked

$$\boxed{\widetilde{F_{mp}} = \varepsilon_{mp}^c \, l_{mp}^c \, \mathcal{F}\left(\overline{u}_m^{c,n}, \overline{u}_p^{v,n}, \boldsymbol{n}_{mp}\right)}$$

5. Through the corrected reconstructed flux, recompute the submean values for tagged subcells and their first neighbors
6. Return to 3

Conclusion

- The correction only affects the DG solution at the subcell scale
- The corrected scheme is conservative at the subcell level
- In practice, few submean values need to be recomputed

Remarks

- For non-linear problems, using very high-order schemes and coarse meshes, the solution may remain a bit oscillatory at the subcell level
- This is why we were previously considering, for $k \geq 3$, that if a subcell is marked as bad then we also mark its first neighboring subcells

F. VILAR, *A Posteriori Correction of High-Order DG Scheme through Subcell Finite Volume Formulation and Flux Reconstruction.* JCP, 2018.

New correction principle

To avoid too much discrepancy between corrected and reconstructed fluxes

- Wider subcell set to be corrected
- Convex combination between 1st-order flux and the reconstructed flux

$$\boxed{\widetilde{F_{mp}} = \theta_{mp}\, \varepsilon^c_{mp}\, l^c_{mp}\, \mathcal{F}\left(\overline{u}_m^{c,n}, \overline{u}_p^{v,n}, \boldsymbol{n}_{mp}\right) + (1-\theta_{mp})\, \widehat{F_{mp}},}$$

where θ_{mp} is a function of the distance to the non-admissible subcell

Corrected reconstructed flux

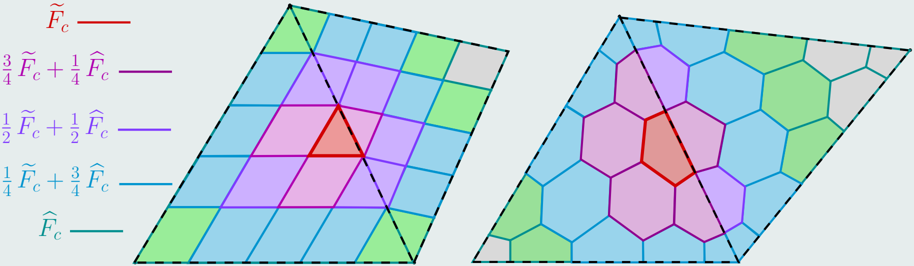

(f) Structured subdivision.

(g) Voronoi-type subdivision.

Figure : New correction of the DG reconstructed flux

Burgers equation with $u_0(x,y) = \sin(2\pi\,(x+y))$

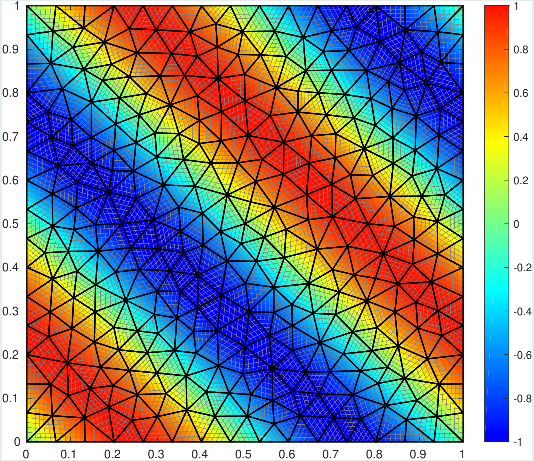

Figure : Entropic weak solution: apparition of stationary shocks

6th-order scheme on a 576 cells grid

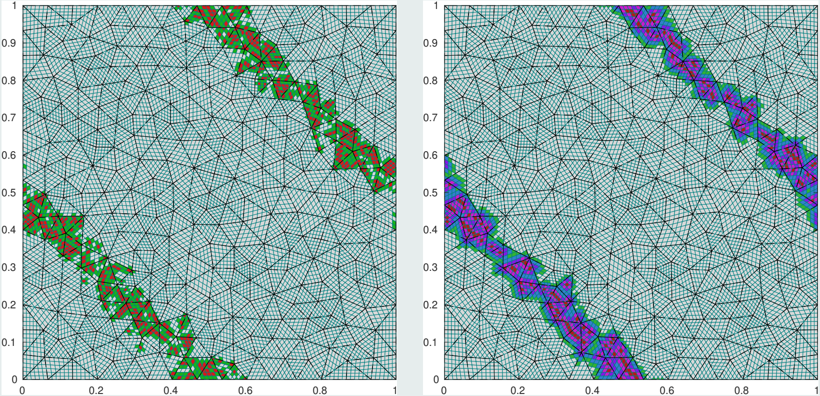

(a) Original correction

(b) New correction

Figure : Comparison between original and new correction procedure: corrected subcells

6th-order scheme on a 576 cells grid - zoom in $[0.65, 0.9]^2$

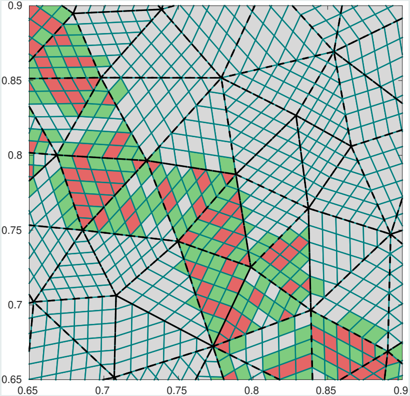

(a) Original correction

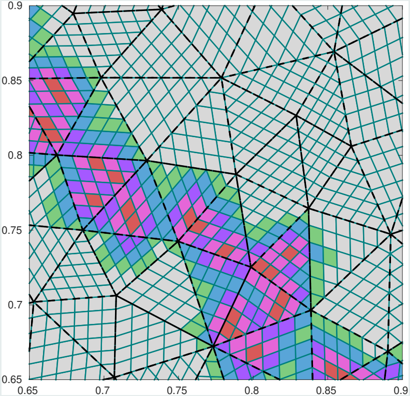

(b) New correction

Figure : Comparison between original and new correction procedure: corrected subcells

6th-order scheme on a 576 cells grid

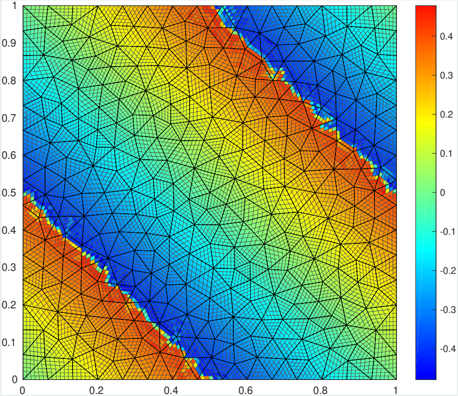

(a) Original correction

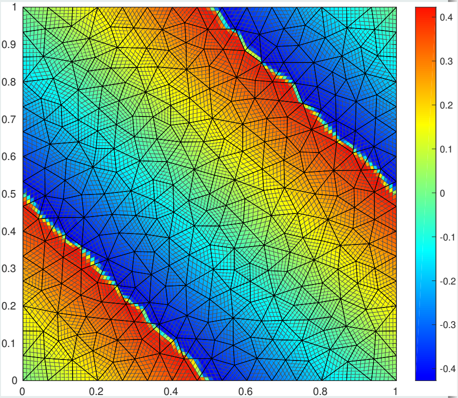

(b) New correction

Figure : Comparison between original and new correction procedure: subcell mean values

6th-order scheme on a 576 cells grid

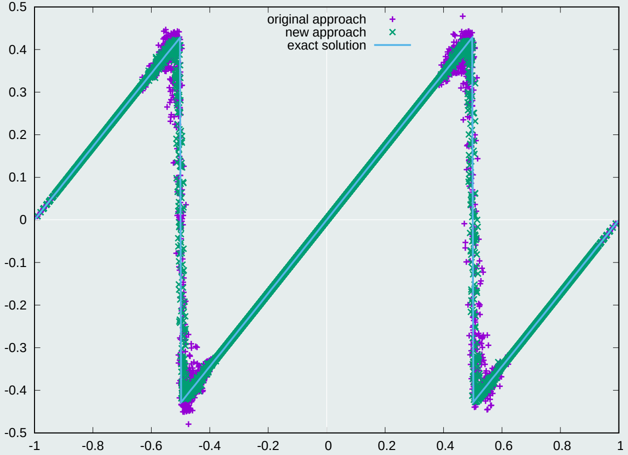

Figure : Comparison between original and new correction procedure: submean values versus $(x + y - 1)$ coordinate

2D Linear advection

- $\partial_t u(\boldsymbol{x},t) + \boldsymbol{A}\,.\,\nabla_x u(\boldsymbol{x},t) = 0$ with $\boldsymbol{A}$ transport velocity

Linear advection of a crenel signal $\boldsymbol{A} = (1,\ 1)^t$

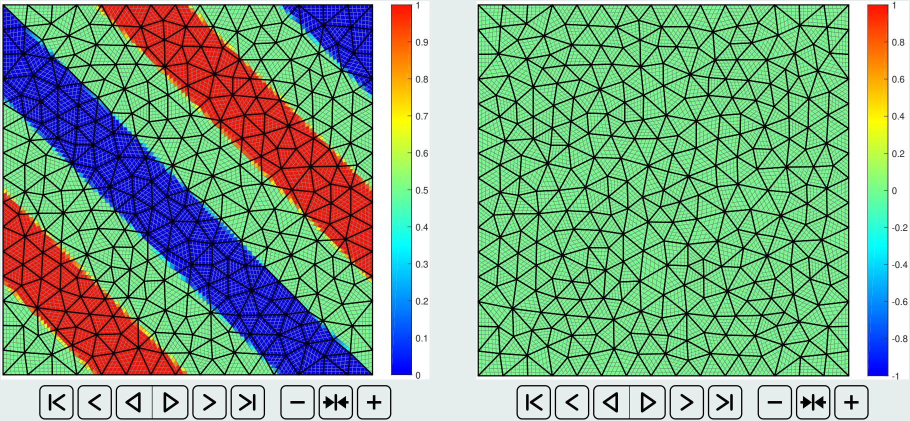

(a) Subcell mean values (b) Corrected subcells

Figure : 6th-order APLSC-DG on a 576 cells mesh after one period

Linear advection equation of a crenel signal $\boldsymbol{A} = (1,\, 1)^t$

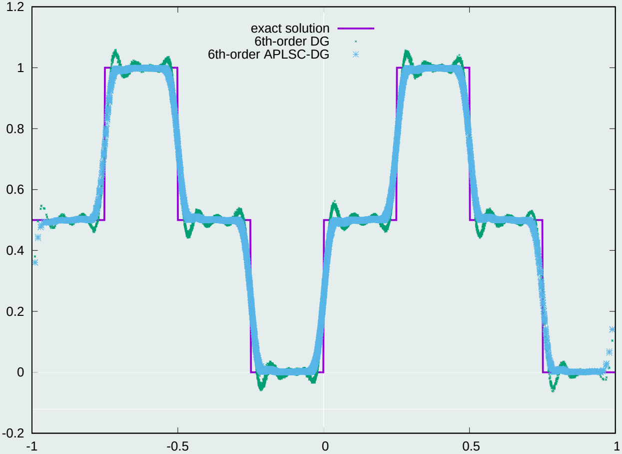

Figure : 6th-order solutions for the crenel advection case on 576 cells: submean values versus $(x + y - 1)$ coordinate

Influence of the subdivision

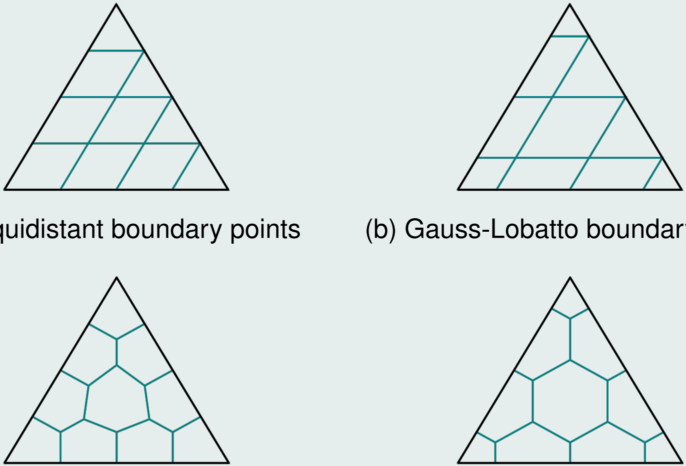

(a) Equidistant boundary points

(b) Gauss-Lobatto boundary points

(c) Equidistant boundary points

(d) $\mathbb{P}^3$ Lagrangian mid-points

Figure : Examples of subdivisions for a triangular cell and a $\mathbb{P}^3$ DG scheme

Linear advection equation of a crenel signal $\boldsymbol{A} = (1,\ 1)^t$

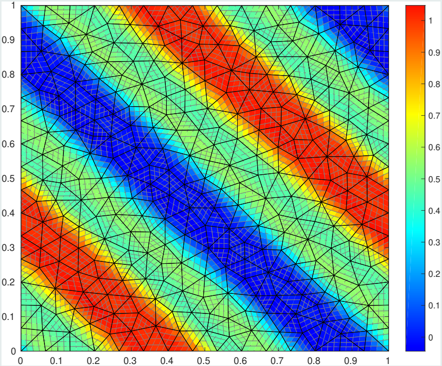

(a) Uniform structured subdivision

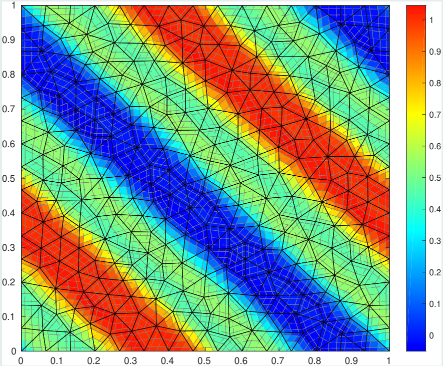

(b) Non-uniform structured subdivision

Figure : 4th-order DG solutions for the crenel signal advection on 576 cells after five periods: structured subdivision

Linear advection equation of a crenel signal $\boldsymbol{A} = (1,\, 1)^t$

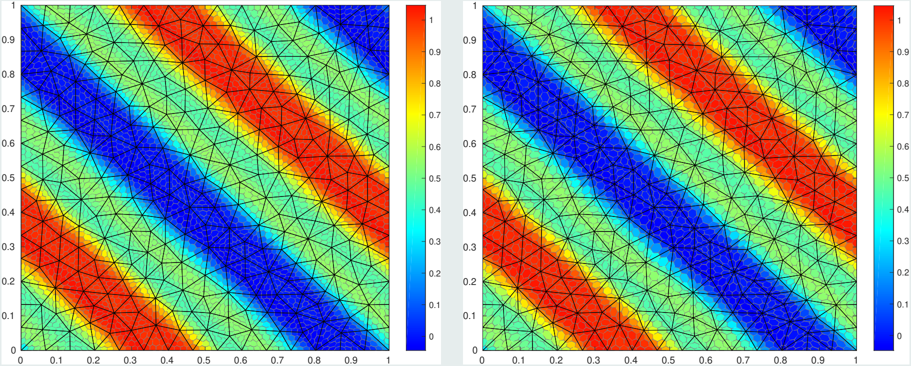

(a) Uniform polygonal subdivision (b) Non-uniform polygonal subdivision

Figure : 4th-order DG solutions for the crenel signal advection on 576 cells after five periods: polygonal subdivision

Linear advection equation of a crenel signal $\boldsymbol{A} = (1, 1)^t$

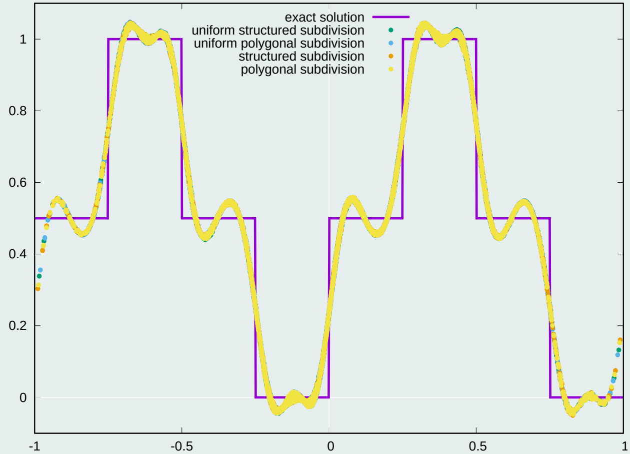

Figure : 4th-order DG solutions for the crenel signal advection on 576 cells using different cell subdivisions: submean values versus $(x + y - 1)$ coordinate

Linear advection equation of a crenel signal $\boldsymbol{A} = (1,\, 1)^t$

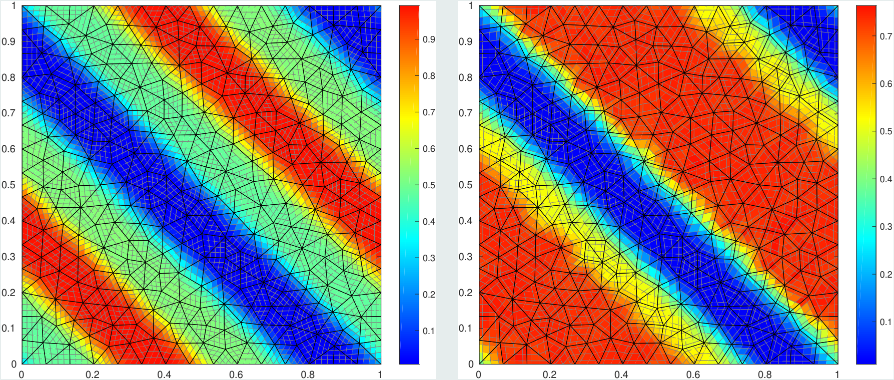

(a) Uniform structured subdivision

(b) Non-uniform structured subdivision

Figure : 4th-order APLSC-DG solutions for the crenel signal advection on 576 cells after five periods: structured subdivision

Linear advection equation of a crenel signal $\boldsymbol{A} = (1,\, 1)^t$

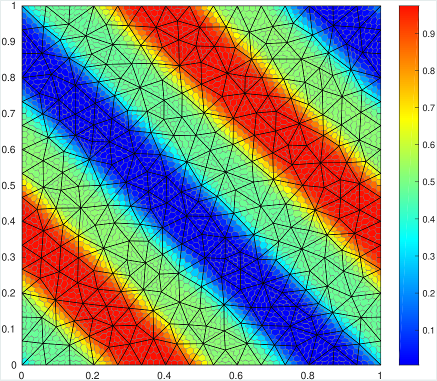

(a) Uniform polygonal subdivision

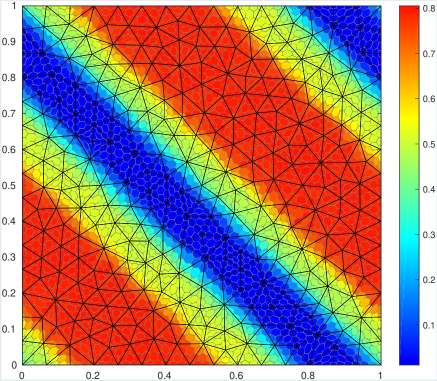

(b) Non-uniform polygonal subdivision

Figure : 4th-order APLSC-DG solutions for the crenel signal advection on 576 cells after five periods: polygonal subdivision

Linear advection equation of a crenel signal $\boldsymbol{A} = (1,\,1)^t$

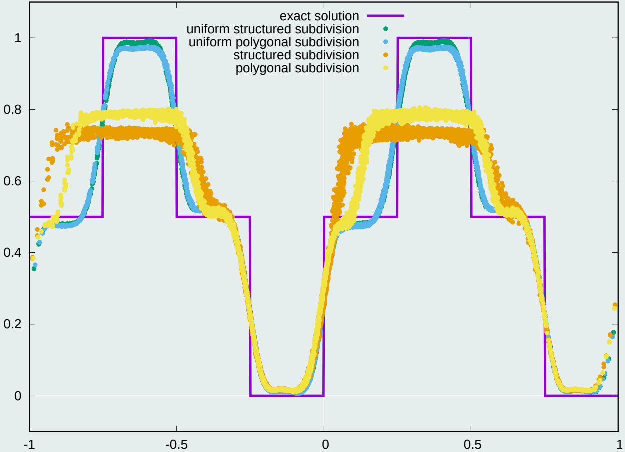

Figure : 4th-order APLSC-DG solutions for the crenel signal advection on 576 cells using different cell subdivisions: submean values versus $(x + y - 1)$ coordinate

2D solid body rotation

- $\partial_t u(\boldsymbol{x}, t) + \boldsymbol{A}(\boldsymbol{x}) \,.\, \nabla_x u(\boldsymbol{x}, t) = 0$ with $\boldsymbol{A}(\boldsymbol{x}) = (0.5 - y,\ x - 0.5)^t$
- $u(\boldsymbol{x}, 0) = u_0(\boldsymbol{x})$

Composite signal rotation: 6th-order APLSC-DG on 576 cells

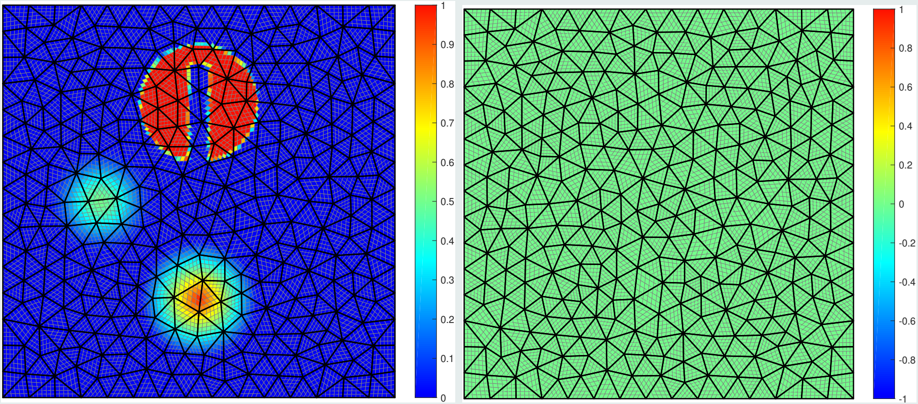

(a) Solution map

(b) Corrected subcells

Rotation of a composite signal after 1 period

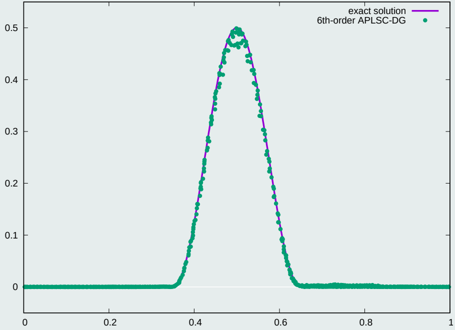

(a) $y = 0.25$

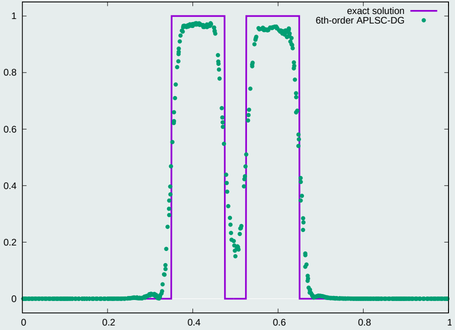

(b) $x = 0.25$

Figure : 6th-order APLSC-DG solution for the rigid rotation case on 576 cells after one full rotation: solution profiles

Rotation of a composite signal after 5 periods

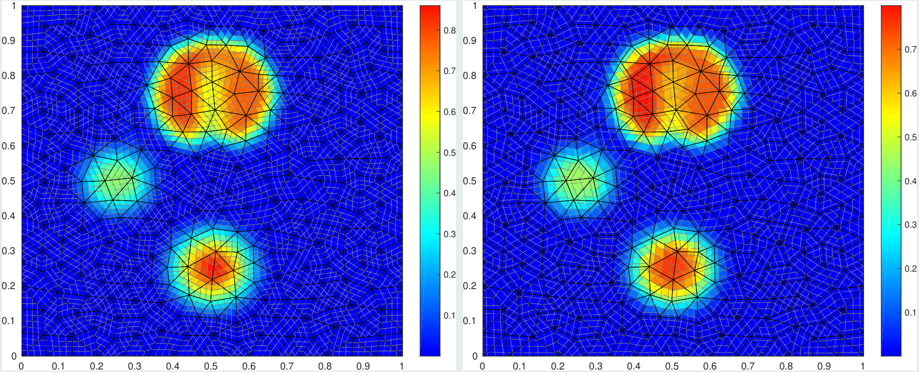

(a) Uniform structured subdivision

(b) Non-uniform structured subdivision

Figure : 4th-order APLSC-DG solutions for the rigid rotation case on 576 cells after five full rotations: structured subdivision

Rotation of a composite signal after 5 periods

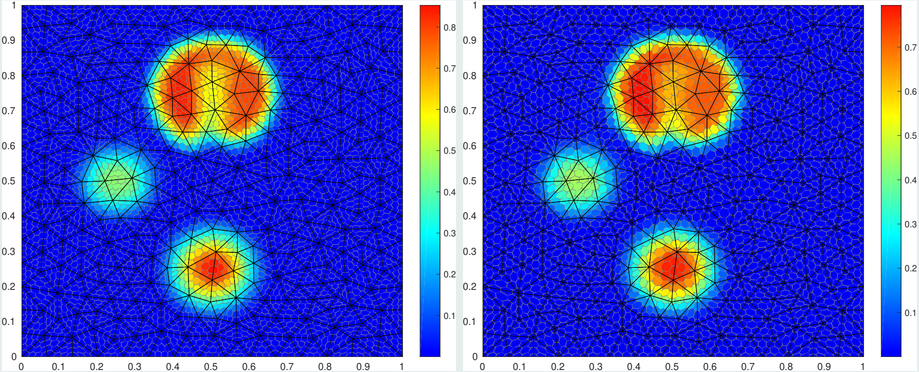

(a) Uniform polygonal subdivision (b) Non-uniform polygonal subdivision

Figure : 4th-order APLSC-DG solutions for the rigid rotation case on 576 cells after five full rotations: polygonal subdivision

Rotation of a composite signal after 5 periods

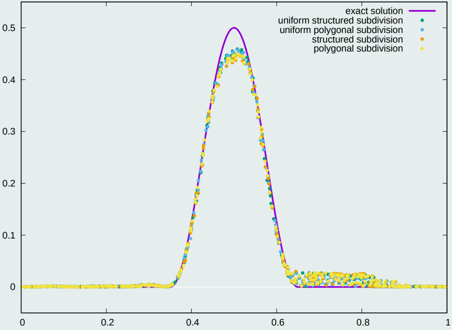

(a) $y = 0.25$

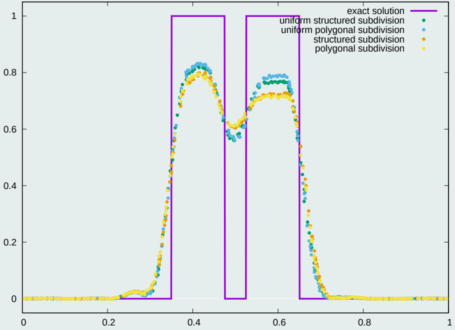

(b) $x = 0.25$

Figure : 4th-order APLSC-DG solutions for the rigid rotation case on 576 cells after five full rotations: solution profiles

2D non-linear Burgers equation

- $\partial_t u(\boldsymbol{x}, t) + \nabla_x \,.\, \boldsymbol{F}\,(u(\boldsymbol{x}, t)) = \boldsymbol{0} \qquad \text{with} \qquad \boldsymbol{F}(u) = \frac{1}{2}\left(u^2,\, u^2\right)^{t}$
- $u(\boldsymbol{x}, 0) = u_0(\boldsymbol{x})$

Burgers equation with $u_0(x, y) = \sin(2\pi\,(x + y))$

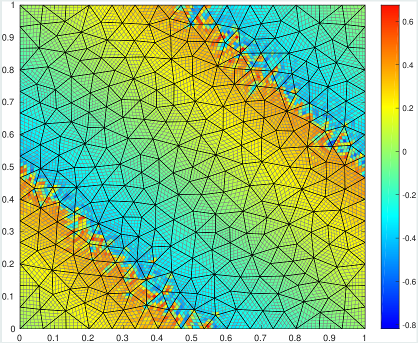

(a) Solution map

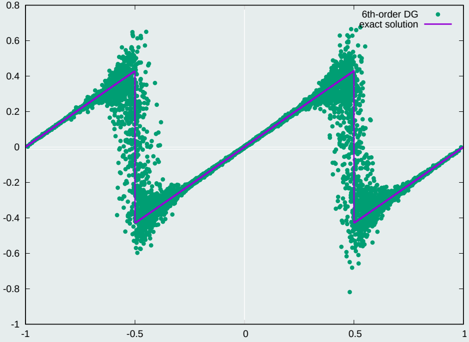

(b) Solution profile

Figure : 6th-order uncorrected DG on a 576 cells mesh at $t = 0.5$

Burgers equation with $u_0(x, y) = \sin(2\pi\,(x + y))$

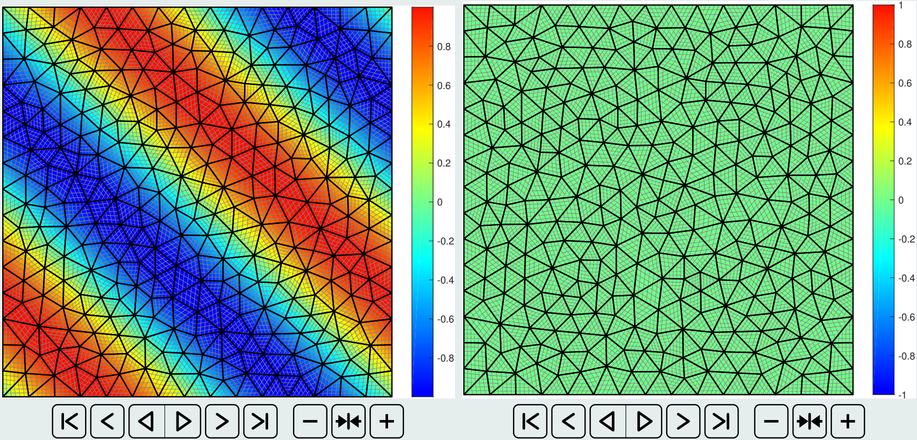

(a) Solution map (b) Corrected subcells

Figure : 6th-order APLSC-DG on a 576 cells mesh at $t = 0.5$

Burgers equation with $u_0(x,y) = \sin(2\pi\,(x+y))$

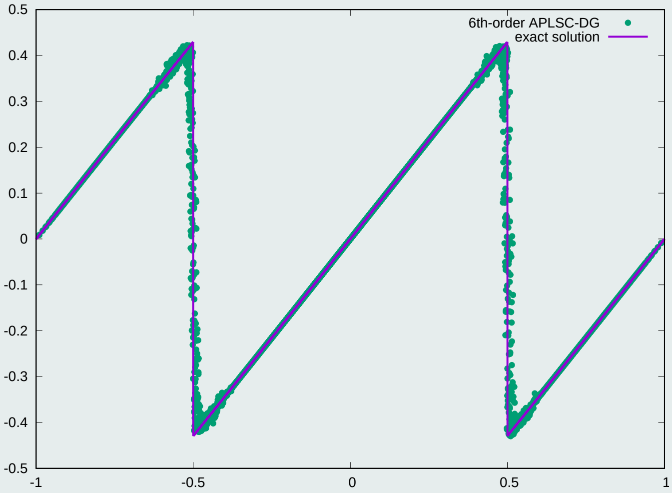

Figure : 6th-order uncorrected DG on a 576 cells mesh at $t = 0.5$: submean values versus $(x + y - 1)$ coordinate

Burgers equation with $u_0(x,y) = \sin(2\pi\,(x+y))$

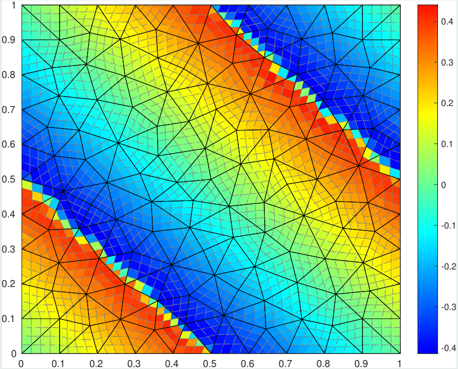

(a) Uniform structured subdivision

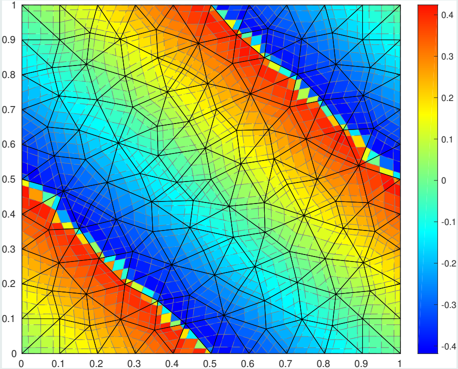

(b) Non-uniform structured subdivision

Figure : 4th-order APLSC-DG solutions for 2D Burgers equation on 242 cells at $t = 0.5$: structured subdivision

Burgers equation with $u_0(x, y) = \sin(2\pi\,(x + y))$

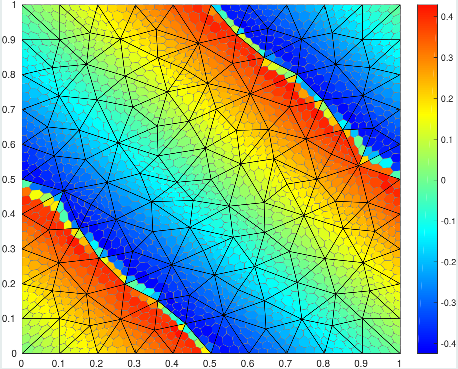

(a) Uniform polygonal subdivision

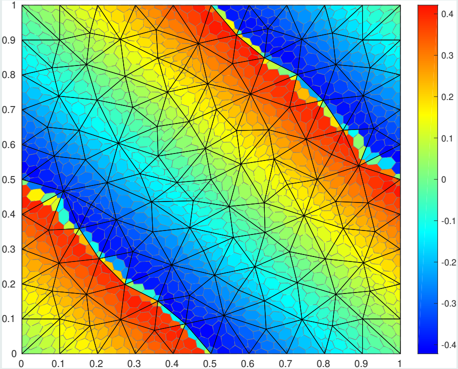

(b) Non-uniform polygonal subdivision

Figure : 4th-order APLSC-DG solutions for 2D Burgers equation on 242 cells at $t = 0.5$: polygonal subdivision

Burgers equation with $u_0(x,y) = \sin(2\pi\,(x+y))$

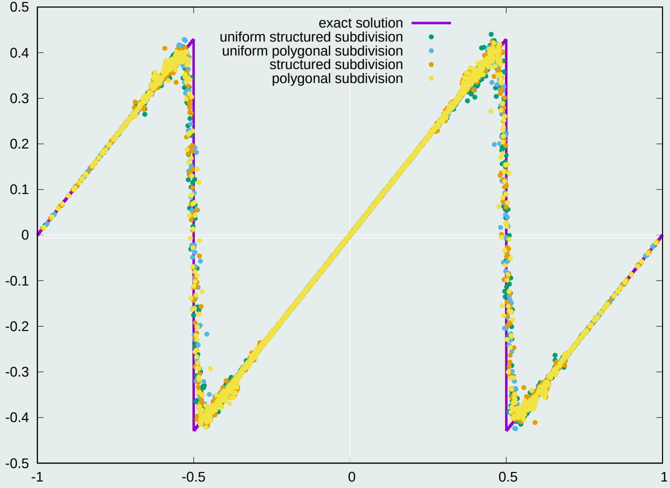

Figure : 4th-order APLSC-DG solutions for 2D Burgers equation on 242 cells at $t = 0.5$: submean values versus $(x + y - 1)$ coordinate

2D Kurganov, Petrova, Popov (KPP) non-convex flux equation

- $\partial_t u(\boldsymbol{x}, t) + \nabla_x \cdot \boldsymbol{F}(u(\boldsymbol{x}, t)) = \boldsymbol{0}$ with $\boldsymbol{F}(u) = (\sin u, \cos u)^t$
- $u(\boldsymbol{x}, 0) = u_0(\boldsymbol{x})$

KPP non-convex flux problem

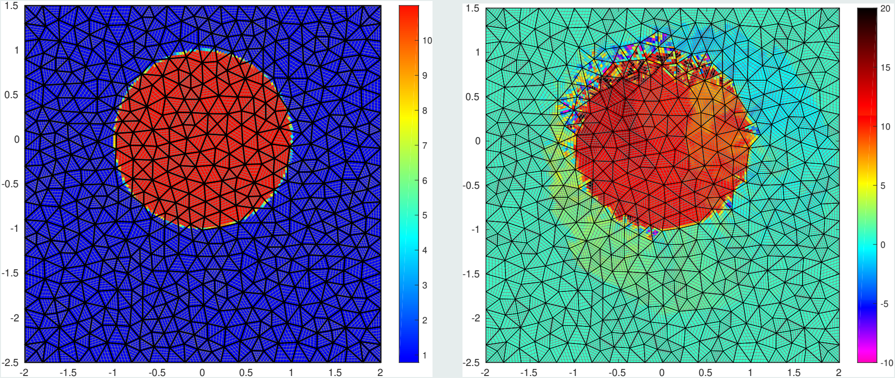

(a) At time $t = 0$

(b) At time $t = 1$

Figure : 6th-order uncorrected DG solution on a 1054 cells mesh

KPP non-convex flux problem

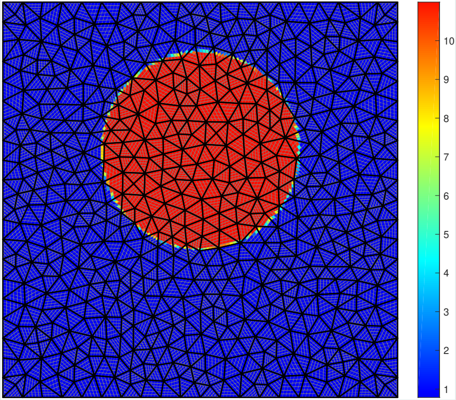

(a) Solution map

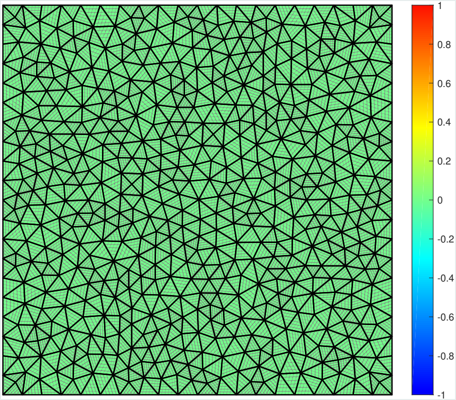

(b) Corrected subcells

Figure : 6th-order APLSC-DG solution on a 1054 cells mesh

KPP non-convex flux problem

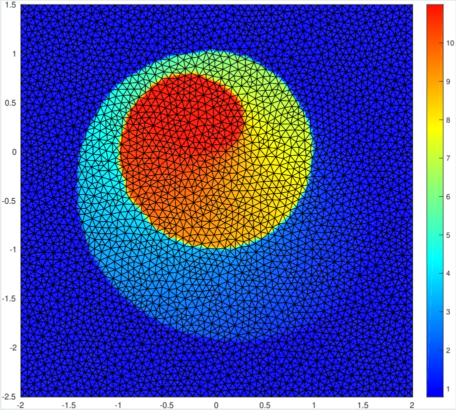

(a) Solution map

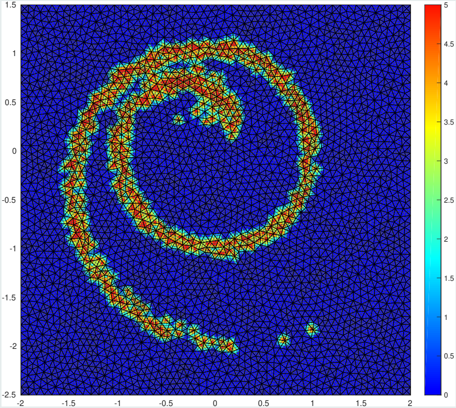

(b) Corrected subcells

Figure : 3rd-order APLSC-DG solution on a 6670 cells mesh

KPP non-convex flux problem

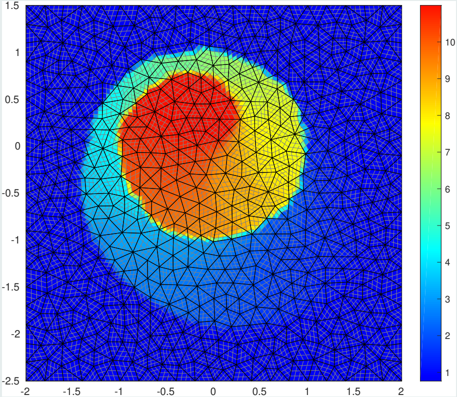

(a) Structured subdivision

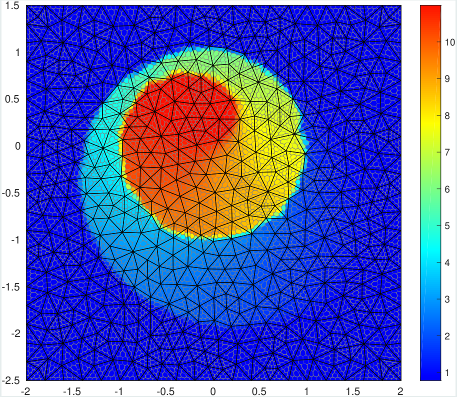

(b) Voronoi-type subdivision

Figure : 4th-order APLSC-DG solution on a 1054 cells mesh: subdivision comparison

2D non-linear Euler compressible gas dynamics equations

- $\partial_t \boldsymbol{V} + \nabla_x \,.\, \boldsymbol{F}(\boldsymbol{V}) = \boldsymbol{0}$

- $\boldsymbol{V} = \begin{pmatrix} \rho \\ \boldsymbol{q} \\ E \end{pmatrix}$ conservative variables

- $\boldsymbol{F}(\boldsymbol{V}) = \begin{pmatrix} \boldsymbol{q} \\ \dfrac{\boldsymbol{q} \otimes \boldsymbol{q}}{\rho} + p\, I_d \\ (E + p)\, \dfrac{\boldsymbol{q}}{\rho} \end{pmatrix}$ flux function

- $p := p(\boldsymbol{V}) = (\gamma - 1)\left(E - \dfrac{1}{2}\, \dfrac{\|\boldsymbol{q}\|^2}{\rho}\right)$ equation of state

APLSC-DG scheme property

- Positivity of the density and internal energy, at the subcell scale

Sod shock tube problem in cylindrical geometry

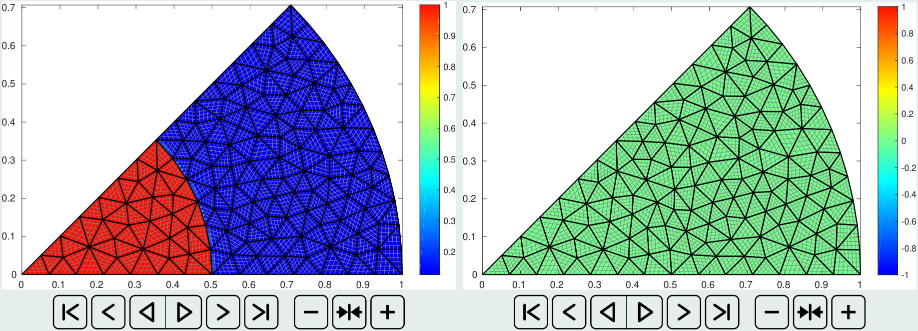

(a) Density map (b) Corrected subcells

Figure : 6th-order APLSC-DG solution on a 230 cells mesh

Sod shock tube problem in cylindrical geometry

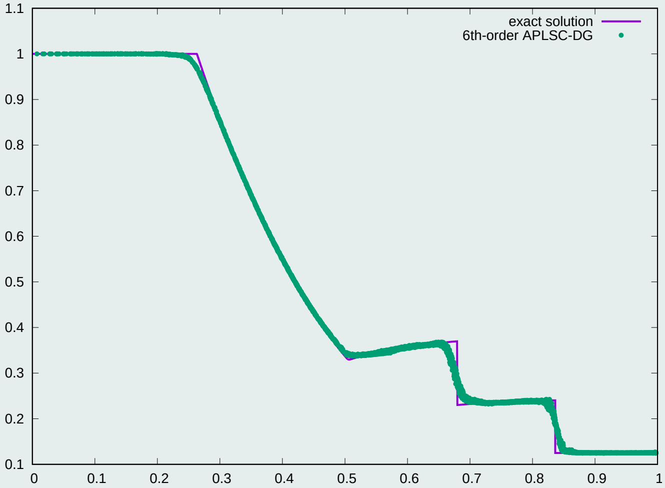

Figure : 6th-order APLSC-DG solution on a 230 cells: density submean values

Sedov point blast problem in cylindrical geometry

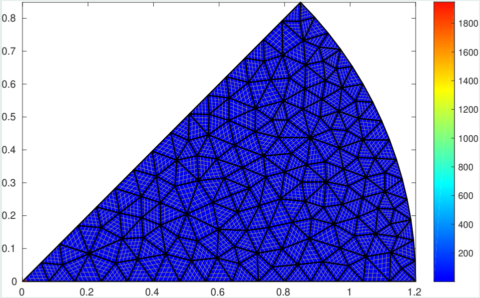

(a) Energy map

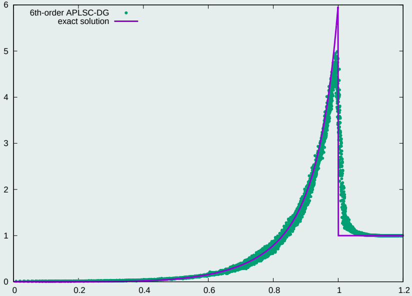

(b) Density profile

Figure : 6th-order APLSC-DG on a 271 cells mesh at $t = 1$

A Mach 3 wind tunnel with a step

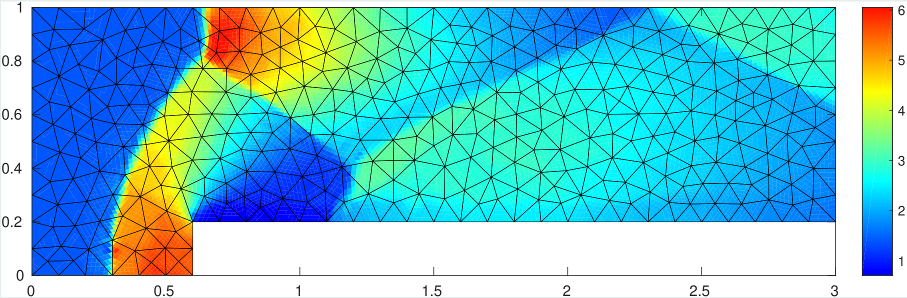

Figure : 6th-order APLSC-DG solution for the facing step problem on 680 cells at $t = 4$: submean density map

2D non-linear shallow water equations - prebalanced formulation

- $\partial_t \boldsymbol{V} + \nabla_x \boldsymbol{.} \boldsymbol{F}(\boldsymbol{V}, b) = \boldsymbol{B}(\boldsymbol{V}, \nabla_x b)$
- $\boldsymbol{V} = \begin{pmatrix} \eta \\ \boldsymbol{q} \end{pmatrix}$ <u>conservative variables</u>
- $\boldsymbol{B}(\boldsymbol{V}, \partial_x b) = \begin{pmatrix} 0 \\ -g\,\eta\,\nabla_x b \end{pmatrix}$ <u>source term</u>
- $\boldsymbol{F}(\boldsymbol{V}, b) = \begin{pmatrix} \boldsymbol{q} \\ \dfrac{\boldsymbol{q} \otimes \boldsymbol{q}}{\eta - b} + \dfrac{1}{2} g\ (\eta^2 - 2\,\eta\, b)\ I_d \end{pmatrix}$ <u>flux function</u>

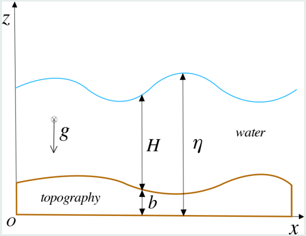

APLSC-DG scheme properties

- Positivity-preservation of the water height $H = \eta - b$, at the subcell scale
- Well-balancing property, at the subcell scale

Well-balancing property

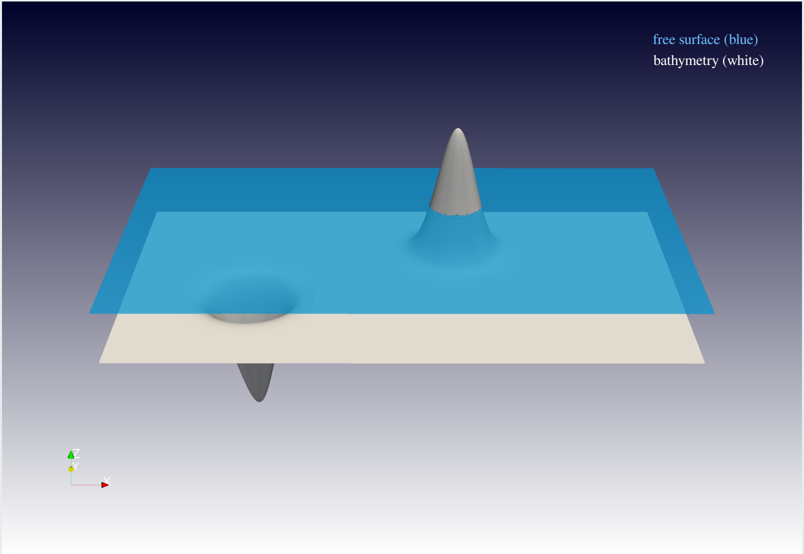

Figure : 3rd-order APLSC-DG on a 5000 cells at $t = 50$: free surface elevation

Dam break problem in cylindrical geometry

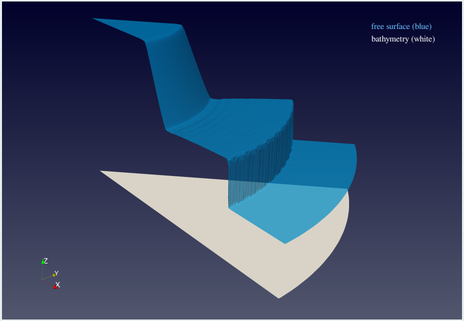

(a) Solution map

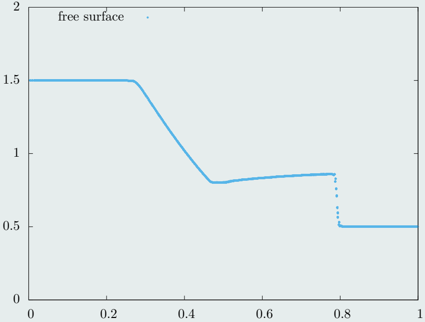

(b) Solution profile

Figure : 3rd-order APLSC-DG on a 2676 cells mesh at $t = 0.045$: free surface elevation

Rock-wave interaction

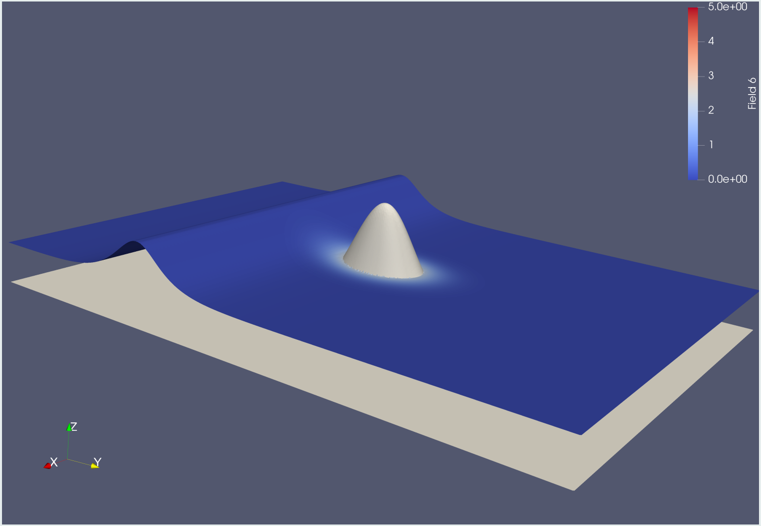

Figure : 3rd-order APLSC-DG on a 7000 cells mesh

A Posteriori Local Subcell Correction (APLSC) technique

- Reformulate DG schemes as subgrid FV-like schemes
- Design an original local subcell correction:
  - preserving the scheme conservation at the subcell scale
  - preserving the very accurate subcell resolution of DG schemes
  - ensuring a maximum or positivity preserving principle at the subcell scale
  - reducing significantly the apparition of spurious oscillations
  - limiting the correction computational effort by not recomputing solution in admissible subcell not lying in the vicinity of a troubled subcell

Applications

- Scalar conservation laws (1D and 2D)
- Euler compressible gas dynamics system (1D and 2D)
- Non-linear shallow water (NSW) system (1D and 2D) **Ali Haidar**
- NSW interactions with a floating object in the arbitrary-Lagrangian-Eulerian (ALE) framework (1D) **Ali Haidar**

Ongoing work

- Application to 2D total Lagrangian hydrodynamics on curvilinear grids
- Maximum principle DG scheme through subcell reconstructed FCT

Future work

- DoF based adaptive DG scheme through subcell Finite Volume formulation in collaboration with **Raphaël Loubère**
- Application to 2D hydrodynamics and solid dynamics in the ALE framework in collaboration with **Walter Boscheri**
- 2D NSW interactions with a floating object in the ALE framework in collaboration with **Fabien Marche**

Articles on this topic

- **F. Vilar**, *A Posteriori Correction of High-Order DG Scheme through Subcell Finite Volume Formulation and Flux Reconstruction.* JCP, 387:245-279, 2018.

- **A. Haidar**, **F. Marche** and **F. Vilar**, *A posteriori Finite-Volume local subcell correction of high-order discontinuous Galerkin schemes for the nonlinear shallow-water equations*. JCP, 452:110902, 2022.

- **A. Haidar**, **F. Marche** and **F. Vilar**, *Nonlinear shallow water interactions with a partially immersed object: a robust high-order DG-ALE formulation*. JCP, **Article under revision**.

- **A. Haidar**, **F. Marche** and **F. Vilar**, *Numerical approximation of nonlinear shallow-water interacting with a floating object*. **Article in preparation**.

- **F. Vilar** and **R. Abgrall**, *A posteriori local subcell correction of DG schemes through Finite Volume reformulation on unstructured grids.* **Article finished, yet to be submitted!!**

Articles on this topic

- **F. Vilar**, *A Posteriori Correction of High-Order DG Scheme through Subcell Finite Volume Formulation and Flux Reconstruction.* JCP, 387:245-279, 2018.

- **A. Haidar**, **F. Marche** and **F. Vilar**, *A posteriori Finite-Volume local subcell correction of high-order discontinuous Galerkin schemes for the nonlinear shallow-water equations*. JCP, 452:110902, 2022.

- **A. Haidar**, **F. Marche** and **F. Vilar**, *Nonlinear shallow water interactions with a partially immersed object: a robust high-order DG-ALE formulation*. JCP, **Article under revision**.

- **A. Haidar**, **F. Marche** and **F. Vilar**, *Numerical approximation of nonlinear shallow-water interacting with a floating object*. **Article in preparation**.

- **F. Vilar** and **R. Abgrall**, *A posteriori local subcell correction of DG schemes through Finite Volume reformulation on unstructured grids.* **Article finished, yet to be submitted!!**

NAD: neighboring subcells set **linear problems**

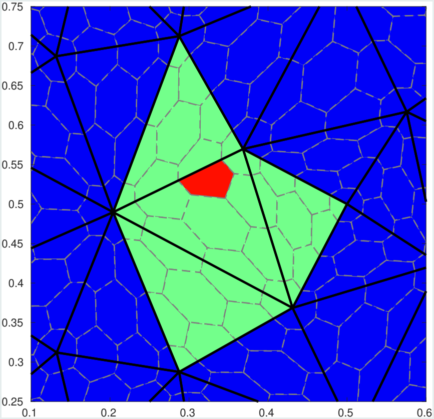

(a) 4th-order, polygonal subdivision

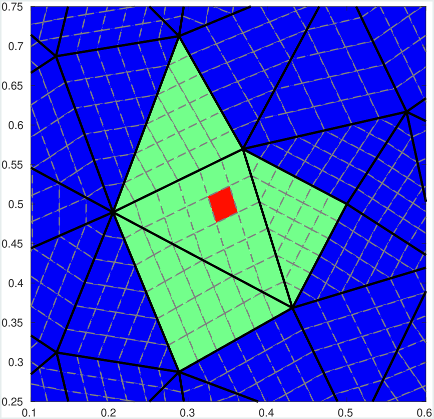

(b) 6th-order, structured subdivision

Figure : Neighboring subcells set for the numerical admissibility criterion

NAD: neighboring subcells set **non-linear problems**

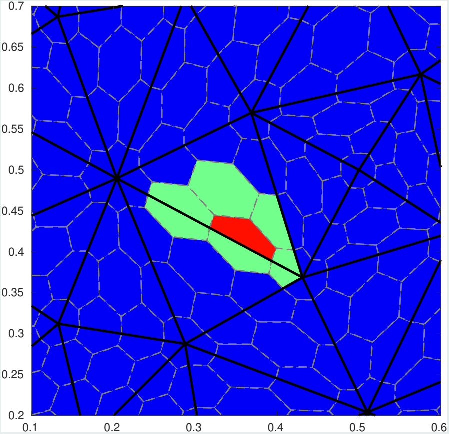

(a) 4th-order, polygonal subdivision

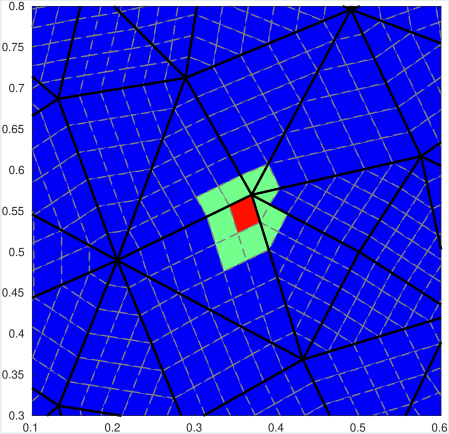

(b) 6th-order, structured subdivision

Figure : Neighboring subcells set for the numerical admissibility criterion

Cell subdivision: condition number of the projection matrix P_c

	$\mathbb{P}^0$	$\mathbb{P}^1$	$\mathbb{P}^2$	$\mathbb{P}^3$
Unif. struct. subdiv.	1	4	10.91	31.75
Non-unif. struct. subdiv.	1	4	9.52	29.28
Unif. polyg. subdiv.	1	2.87	8.73	27.89
Non-unif. polyg. subdiv.	1	2.87	8.19	26.94

Table: Projection matrix condition number for different orders and subdivisions